Expression of thioredoxin-1 in the ASJ neuron corresponds with and enhances intrinsic regenerative capacity under lesion conditioning in *C. elegans*

Noa W.F. Grooms, Michael Q. Fitzgerald, Leilani G. Schulting, Samuel E. Ureña, Samuel H. Chung

Abstract

A conditioning lesion of the peripheral sensory axon triggers robust central axon regeneration in mammals. We visualize the ASJ neuron of *C. elegans* with a cell-specific green fluorescent protein reporter driven by a thioredoxin *trx-1* promoter and trigger conditioned regeneration by laser surgery or genetic disruption of sensory pathways. Utilizing calibrated fluorescent beads, we demonstrate that these neurons brighten when conditioned, suggesting that *trx-1* expression indicates regenerative capacity. We show that *trx-1* functionally enhances conditioned regeneration but inhibits non-conditioned regeneration. Finally, six strains isolated in a forward genetic screen for reduced fluorescence also show reduced axon outgrowth. We demonstrate a link between *trx-1* expression and the conditioned state that we leverage to rapidly assess regenerative capacity.

Keywords

neuron regeneration; lesion conditioning; thioredoxin; genetic screen; *C. elegans*; fluorescence microscopy

Abbreviations

CNS, central nervous system; EMS, ethyl methanesulfonate; DLK, dual-leucine kinase; TXN, thioredoxin; cAMP, cyclic adenosine monophosphate; CRE, cAMP responsive element; RAG, regeneration associated gene; RNAi, ribonucleic acid interference; a+d, axon + dendrite surgery

Introduction

The exquisitely complex and precise shape of neurons makes them highly susceptible to injury and disease. Compounding this weakness is the extremely limited regenerative capacity of the mammalian central nervous system (CNS), which severely limits functional recovery. Millions of people worldwide are affected by traumatic brain or spinal cord injury, amyotrophic lateral sclerosis (ALS), Alzheimer's, Parkinson's, or other neurodegenerative disorders (Feigin*, et al.*, 2021; James*, et al.*, 2019). The lack of effective treatments for these afflictions represents one of the areas of greatest need in modern medicine.

In a remarkable phenomenon known as lesion conditioning, damage to a neuron's peripheral sensory fiber triggers cellular mechanisms to drive regeneration in the CNS (McQuarrie and Grafstein, 1973; Richardson and Issa, 1984). Lesion conditioning fosters a pro-regenerative environment (Dubový*, et al.*, 2019; Xiong and Collins, 2012), enhances neuroregeneration (Hoffman, 2010) by overcoming CNS inhibitory growth cues (Chong*, et al.*, 1996; Oudega*, et al.*, 1994), and even dramatically reduces neurodegenerative markers in disease models (Franz*, et al.*, 2009). Therefore, lesion conditioning drives and enables regeneration that could treat CNS afflictions.

Our laboratory utilizes the roundworm *Caenorhabditis elegans* for their strongly conserved genetics with mammals, facile genetics, optical transparency, and rapid development. In a prior study, we established a lesion conditioning model in the ASJ sensory neuron (Chung*, et al.*, 2016). We discovered that mutation or pharmacological inhibition of genes in sensory transduction pathways can trigger conditioned regeneration, similar to the effect of a conditioning lesion. As shown in Tab. 1, these

interventions produce several observable phenotypes, including conditioned regeneration and a form of ectopic axon outgrowth that has the same underlying genetic pathway.

In this prior study, we cell-specifically labelled the ASJ using a transgenic green fluorescent protein (GFP) reporter driven by a promoter of *trx-1*, which is thioredoxin-1, an ortholog of human thioredoxin, TXN. We noticed by eye that interventions that condition the ASJ also brighten the neuron, indicating an upregulation of the gene driving our fluorescent label. Our visual observations are consistent with prior studies. Following peripheral nerve axotomy, TXN accumulates in the nucleus and dramatically increases throughout the cytoplasm (Mansur*, et al.*, 1998), indicating that it is a regeneration-associated gene (RAG) (Ma and Willis, 2015).

In this study, we quantify ASJ fluorescence and utilize it as an indicator of regenerative capacity. We quantitatively show that mutations that condition the ASJ by disrupting sensory signaling significantly brighten the neuron. Similarly, conditioning by lesion via laser surgery results in significantly increased fluorescence. The intensity of fluorescence following these interventions roughly corresponds with the neuron's regenerative capacity. Additionally, we show that the *trx-1* gene restrains non-conditioned regeneration and enhances conditioned regeneration. We leverage our fluorescent proxy to screen for mutations that underlie conditioning in the ASJ neuron. We isolate twelve mutant lines, spanning six putative mutations, with significantly reduced ASJ fluorescence. Six of these lines also display reduced ectopic outgrowth, indicating a disruption in the conditioning pathway. Our proxy enables efficient isolation

of genes underlying lesion conditioning by enabling a visually-based screen that does not require time-consuming surgery.

Materials and methods

C. elegans cultivation, strains, and mutagenesis: We followed established procedure for cultivation on agarose plates with OP50 bacteria at 20°C (Brenner, 1974). For fluorescent bead measurements, we cultivated animals on Bacto agarose plates at 20°C for multiple generations. We cultivated animals on Difco agarose plates at 20°C and 25°C for laser surgeries and ectopic outgrowth experiments, respectively. We confirmed the genotypes for all mutant strains by polymerase chain reaction followed by Sanger sequencing through GENEWIZ (for single-nucleotide polymorphisms) or gel electrophoresis (for large deletions). Tab. 2 lists the genetics of the strains utilized. We followed established protocol for ethylmethanesulfonate (EMS) mutagenesis (Brenner, 1974).

Laser surgery, imaging of axon regrowth and ectopic outgrowth, and postprocessing: We followed established procedures for animal immobilization by sodium azide (Chung*, et al.*, 2006) and femtosecond laser surgery (Harreguy*, et al.*, 2020; Wang*, et al.*, 2022). We severed only the axon (within 2 μm from the cell body), only the dendrite (2/3rd the length distal from the cell body), or both the axon and dendrite (axon+dendrite), and we reimaged 48 hours afterwards. We followed established procedures for immobilizing animals on agarose-azide pads, imaging axon growth, and postprocessing images to measure regenerated length (Chung*, et al.*, 2016).

Imaging with fluorescent beads: Fluorescence measurements are affected by numerous factors, including the intensity of the light source and transmission through microscope optics. These factors may change over time as the components age and their alignment degrades. To account for these effects, we calibrated fluorescence measurements by imaging animals alongside fluorescent beads and normalizing measurements across the images taken. We thoroughly vortexed 0.3% and 3% 2.5 μm stock bead solution (Invitrogen I7219) and mixed it with nematode growth medium (NGM) buffer (Chung*, et al.*, 2016) in a 5:1 NGM to bead volumetric ratio. We dropped 5.0 μL of the 5:1 solution to the center of the agarose-azide pad, and then picked adults to the bead solution droplet. To approximately match neuron to bead fluorescence, we used 3% beads for *tax-2* and *tax-4* strains and 0.3% beads for other strains and surgical conditions. We imaged worms through a Nikon 0.30 NA, 10x microscope objective and an Andor Zyla sCMOS Plus camera. Z-stack images were captured with 1-μm spacing.

Postprocessing of fluorescence measurements: We create maximum intensity projections of our raw z-stack images in ImageJ and identify the brightest pixel within the ASJ cell body and dendrite for each animal. The pixel values are the raw fluorescent intensities. Additionally, we average the brightest pixel value within five representative beads in each raw image. We normalize and scale all raw neuron intensities to our reference (*tax-2*) intensities according to equation (1):

(1) $$F_{normalized} = F_{raw} * \frac{\bar{F}_{ref\ bead}}{\bar{F}_{raw\ bead}} * \frac{F_{raw\ bead\ type}}{F_{ref\ bead\ type}}$$, where,

F_{raw} is raw fluorescent intensity of ASJ cell body or dendrite.

$\bar{F}_{raw\ bead}$ is the average of the fluorescence intensity of five representative beads in the raw image.

$\bar{F}_{ref\ bead}$ is average of the fluorescence intensity of all representative beads in the set of reference images.

$\frac{F_{raw\ bead\ type}}{F_{ref\ bead\ type}}$ is the true ratio of bead fluorescent intensities according to manufacturer data. This ratio is 0.08 if the raw image is calibrated with 0.3% beads or 1.00 if calibrated with 3% beads like the reference image.

The first ratio of Eq. (1) normalizes for day-to-day variability in imaging parameters between an image and the reference image set. If beads appear unusually bright in an image due to stronger illumination or increased transmission, then this ratio will compensate. If the beads are abnormally dim, the opposite will occur. The second ratio compares the expected brightness of the bead type used in the image against the reference bead type. Under ideal imaging conditions, this second ratio comparing the bead intensities from manufacturer data should be the inverse of the first ratio that compares the measured bead intensities. Therefore, the product of the two ratios should center around 1.0 if the bead intensities match their manufacturer specifications.

Statistics and interpretation of results: For axon length and fluorescence measurements, we calculated *P* values by the unpaired, unequal variance, two-tailed *t* test. The conditioning effect is the difference between regenerated length after axon cut and after axon+dendrite cut. Its standard deviation is the square root of the sum of the squares of the regenerated length standard deviations. To compare conditioning effects

in different backgrounds, we calculated *P* values by the unpaired, unequal variance, two-tailed *t* test. To compare frequencies of ectopic outgrowth, we used Fisher's exact test.

Results

Defects in sensory transduction upregulate *trx-1* expression in the ASJ neuron.

The ASJ is an amphid sensory neuron located in the nose of *C. elegans* (Fig. 1a, left). The amphids are bilateral, bipolar neurons following a stereotyped morphology consisting of a cell body, a sensory dendrite that extends to the nose, and an axon that mediates synaptic connections in the nerve ring (White*, et al.*, 1986). The ASJ axon regenerates when it is severed. Mutation of dual-leucine kinase, *dlk-1*, completely abolishes what we call "conventional" (*i.e.*, single-axotomy) axon regeneration (Chung*, et al.*, 2016). The regeneration of other *C. elegans* (Ghosh-Roy*, et al.*, 2010; Hammarlund*, et al.*, 2009) and mammalian neurons (Itoh*, et al.*, 2009; Shin*, et al.*, 2012) also show a strong dependence on *dlk-1*. We trigger DLK-independent regeneration by concomitantly severing the ASJ axon and dendrite. This DLK-independent regeneration exhibits several hallmarks of lesion-conditioned regeneration. We also uncovered several sensory mutations that significantly reduce ASJ neuronal activity levels and thus condition the ASJ to regenerate in *dlk-1* mutants without a physical lesion (Chung*, et al.*, 2016).

We characterized the effect of these mutations on the expression of *ptrx-1::trx-1::gfp* translational fusion reporters *ofIs1* and *ofIs4*. The loci of crucial genes *egl-19* and *unc-43* are on chromosome IV close to the integration site of *ofIs1*, which necessitated the

use of *ofIs4*. While our previous study utilized an extrachromosomal array reporter, *ofIs1* and *ofIs4* are integrated into the genome, allowing more accurate comparison of expression levels across animals. We generated fluorescent animals with the mutations (Fig. 1a) and measured brightness of the ASJ cell bodies and dendrites to roughly assess TRX-1 levels and localization at a subcellular level (Fig. 1b). Scattered and out-of-focus light from the larger, brighter cell body often hides fine or dim structures nearby. Thus, we were unable to consistently measure the intensity of the axon. In wild-type (wt) animals, the ASJ cell body and dendrite are relatively dim. In a *dlk-1* mutant background, the ASJ fluorescence remains dim with a slight decrease in cell body fluorescence ($p < 0.001$), consistent with a non-conditioned regenerative state. The remainder of the mutations significantly increase the brightness of the ASJ fibers and especially cell bodies ($p < 0.001$ for all mutations). The most dramatic alteration in fluorescent intensity occurs under *tax-2* and *tax-4* (Fig. 1b, $p < 0.001$), which also produce the strongest conditioned regeneration of the sensory mutations we studied. The fluorescence in the dendrites of each conditioned strain significantly increase except for *unc-36*, which may be consistent with the weaker conditioning effect of *unc-36* (Chung*, et al.*, 2016). Thus, the expression of *ptrx-1::trx-1::gfp* in the ASJ generally corresponds with regenerative potential but is not predictive at a single gene level.

Dendrite cuts upregulate *trx-1* expression and stimulate *dlk*-independent regeneration in the ASJ neuron.

We also examined changes in ASJ fluorescence in *dlk-1* mutant two days after cutting the axon, dendrite, or axon and dendrite concomitantly (denoted as “axon+dendrite” or

"a+d"). Figure 2a shows images of the ASJ in *dlk-1* animals 48 hours after surgery as well as in a chronically conditioned background, *tax-2*, to represent a strongly conditioned fluorescence level. Figure 2b shows the measured cell body and dendrite fluorescent intensities after each surgery. Figure 2c scatter plots the dendrite fluorescence against the cell body fluorescence, clustering neurons by fluorescent intensity for comparing to conditioned state. Our imaging procedure without surgery (mock condition) does not significantly alter fluorescence, and the data points are tightly clustered on the left side of the plot (dimmer ASJ fluorescence), representing a non-conditioned state. Surgical interventions significantly increase cell body and dendrite fluorescence. Changes in fluorescence after axon cut follow a roughly binary distribution where half remain as dim as the ASJ in mock animals and the other half noticeably brighten. Figure 2c clarifies that the cell body and the dendrite fluorescent intensities after axon cut are correlated, leading to a clear demarcation between non-conditioned and conditioned states. Severing the dendrite or axon+dendrite significantly increases ASJ fluorescence ($p < 0.001$) of nearly the entire population to a brightness that begins to approach the level in *tax-2* animals (right side, Fig. 2b). Figure 2c confirms that neurons are strongly brightened following dendrite and axon+dendrite surgeries. The heightened levels of fluorescent intensity following dendrite or axon+dendrite cut are consistent with these interventions' abilities to condition the neuron to regenerate. The fluorescence after axon+dendrite surgery is not significantly different from after dendrite surgery ($p = 0.163$), suggesting that cutting the dendrite is sufficient for activating the conditioning response. These results are consistent with published findings that TXN

upregulates following peripheral axon injury, the hallmark of a RAG (Bai*, et al.*, 2003; Mansur*, et al.*, 1998).

Postsurgery regenerated length in ASJ expressing *ofIs1* match regeneration under a different translational reporter (Chung*, et al.*, 2016). Conventional regeneration in the ASJ is largely *dlk*-dependent. Figure 2d displays length regenerated by the ASJ in wild-type and *dlk-1* following axotomy or axon+dendrite cut. The ASJ regenerates 43 μm on average following axotomy in wild-type but does not regenerate in *dlk-1* ($p < 0.001$). Because *dlk-1* eliminates conventional ASJ regeneration, it exposes regeneration due to conditioning. Thus, we associate regeneration in *dlk-1* with conditioned regeneration. Note also that while axotomy alone does not produce conditioned regeneration in *dlk-1*, it significantly increases fluorescence of some neurons. This divergence indicates that the fluorescent reporter does not fully indicate the conditioned regenerative state and that *trx-1* expression alone is not sufficient for activating conditioned regeneration. We speculate that the significant increase in fluorescence after axotomy alone could be an upregulation of *trx-1* in response to neuroinjury without activating conditioning mechanisms. The conditioning effect is fundamentally the increase in regeneration arising from a dendrite cut, indicated by the arrows in the figure. Under our model, axon+dendrite cut triggers conventional and conditioned regeneration, which both contribute to the total length.

Opposite effects of *trx-1* on two forms of ASJ regeneration

Given that TXN is a RAG (upregulated following neuron injury), we wanted to determine if *trx-1* is involved in either form of regeneration. Our prior work utilized a

translational *ptrx-1::trx-1::gfp* fusion marker, potentially resulting in an overexpression of functional TRX-1 protein in the ASJ. Therefore, we visualized the ASJ with a transcriptional marker *ofIs5[ptrx-1::gfp]* and probed the effects of *trx-1(ok1449)*, which is a loss-of-function allele deleting a 860 bp region spanning part of the proximal promoter region up to the last exon (Miranda-Vizuete*, et al.*, 2006). As shown in Fig. 3, the trends in regeneration in wild-type and *dlk-1* are consistent with regeneration under translational fusion reporters in Fig. 2 and in our prior study (Chung*, et al.*, 2016). In wild-type animals, the axon regenerates at a basal rate when it is severed, and mutation of *dlk-1* eliminates conventional regeneration. The addition of a dendrite cut increases regeneration in wild-type ($p < 0.05$) and restores regeneration in *dlk-1* due to the conditioning effect ($p < 0.001$).

ASJ conventional regeneration in *trx-1* is significantly stronger than in wild-type ($p < 0.001$). The increased regeneration in *trx-1* following axotomy indicate that *trx-1* restrains conventional regeneration in the ASJ. Introducing the *dlk-1* mutation to *trx-1* mutant background nearly eliminates conventional regeneration (Fig. 3), similar to results in translational fusions and *trx-1(+)*. The conditioning effect in *dlk-1; trx-1* is significantly less than the conditioning effect in *dlk-1*, as indicated by the arrows in Fig. 3 ($p < 0.05$). This indicates that *trx-1* enhances conditioned regeneration.

Screening of *trx-1* reporter isolates mutants with reduced regenerative potential.

One powerful technique for exposing genes underlying a phenotype is the unbiased forward screen (Brenner, 1974). In brief, a screen stochastically introduces mutations into the genomes of many animals. The correlation between *trx-1* expression and

regenerative capacity suggests that we can rapidly screen for genes involved in conditioned regeneration utilizing a *trx-1* fluorescent reporter. We exposed our chronically conditioned *tax-2* strain, labeled with *ofIs1*, to ethyl methanesulfonate (EMS). Starting in the F_2 generation, we isolated mutant lines by visually screening for decreased fluorescence in the ASJ neuron by eye (Fig. 4a) which potentially indicates a defect in a conditioning-related gene. Often, it was difficult to detect a significant reduction in cell body fluorescence, so we screened for significantly dimmer dendrites that we could not observe at a set magnification. We generated twelve mutant lines, spanning six putative mutations, with significantly reduced ASJ fluorescence in the cell body (Fig. 4b) or dendrite (Fig. 4c). Ten of these lines display significantly reduced fluorescence in both the dendrite and cell body ($p < 0.001$).

Mutations to genes involved in the sensory pathways (*i.e.*, conditioning mutations) decrease ASJ neuronal activity and trigger regeneration. These sensory mutations, including the mutations in Fig. 1, also alter axon morphology in *C. elegans* sensory neurons and produce ectopic outgrowths (Coburn and Bargmann, 1996; Peckol*, et al.*, 1999). We found that ectopic outgrowth extensively shares genetic and molecular mechanisms of axon growth with conditioned regeneration (Chung*, et al.*, 2016). Thus, ectopic outgrowth is an indicator of conditioned regenerative potential. As shown in Fig. 4d, six of the strains we isolated exhibit significantly reduced frequencies of ectopic outgrowth compared to the original pre-mutagenized strain ($p < 0.05$ *or* 0.001), suggesting that these strains possess a mutation that restrains conditioned regeneration in the ASJ. As we previously found, fluorescence is not always an accurate predictor of conditioned outgrowth. We identified some strains with significantly reduced cell body

and dendrite fluorescence but unchanged ectopic outgrowth frequency. We expect these strains to carry a mutation that decreases *trx-1* expression without impact to the conditioning pathway. In summary, our results demonstrate the utility and limitations of our fluorescence proxy as an indicator of ASJ intrinsic regenerative capacity.

Discussion

The change in expression of TXN following neuronal injury has been widely characterized in mammalian models. TXN induction occurs after a variety of insults, including ischemia (Tomimoto*, et al.*, 1993) and oxidative stress (Sugino*, et al.*, 1999). Importantly, motor and sensory nerve axotomy in rats leads to significantly increased levels of TXN (Mansur*, et al.*, 1998; Stemme*, et al.*, 1985). Likewise, we note that laser surgery of the ASJ neurites upregulates *trx-1* expression, as indicated by *trx-1::gfp* reporter. Our study offers three lines of evidence for associating this enhanced *trx-1* expression with the conditioned state. First, changes due to conditioning, including upregulation of RAGs, preferentially occurs after lesioning the sensory neurite rather than the central, or synaptic, neurite. In the ASJ neuron, severing the sensory dendrite strongly upregulates *trx-1* in nearly all neurons while severing the axon upregulates only 50% of neurons to a lesser degree (Fig. 2b). Second, each tested mutation that conditions the ASJ neuron to improve regeneration (Chung*, et al.*, 2016) also upregulates expression of *trx-1* (Fig. 1b). Third, *trx-1* expression generally corresponds with conditioned regenerative potential (Fig. 1b). Out of the mutations tested, the *tax-2* and *tax-4* mutations brighten the ASJ the most and produce the highest levels of ectopic outgrowth and regeneration (Chung*, et al.*, 2016). However, this relationship is not

comprehensive. The *tax-2* and *tax-4* mutations produce marginally better conditioned regeneration compared to other mutations, and the *unc-36* mutation increases *trx-1* expression but minimally triggers regeneration (Chung*, et al.*, 2016). This differential alteration of *trx-1* expression and regeneration suggests a divergence of pathways underlying *trx-1* expression and conditioning.

To our knowledge, the role of *trx-1* in neuronal regeneration has not directly been studied, although prior evidence suggests its role as a mediator. Overexpressing TXN in mice can promote neuroprotective effects following stroke (Takagi*, et al.*, 1999), and TXN is required for nerve growth factor enhancement of nerve outgrowth in a tumor cell line (Bai*, et al.*, 2003). We directly test the role of *trx-1* in modulating conventional and conditioned regeneration in the ASJ (Fig. 3). We show that *trx-1* inhibits conventional regeneration, consistent with findings in the PLM sensory neuron in *C. elegans*. Animals defective in thioredoxin reductase *trxr-1*, which enables *trx-1* activity (Stenvall*, et al.*, 2011), display increased PLM regrowth (Kim*, et al.*, 2018). We also show that *trx-1* mediates *dlk*-independent conditioned regeneration, consistent with the upregulation of *trx-1* expression following conditioning interventions. The *trx-1* gene contains a regulatory region with cAMP responsive element (CRE) through which nerve growth factor acts to induce nerve outgrowth (Bai*, et al.*, 2003). The cAMP pathway is one of the best-described mechanisms for enhancing conditioned regeneration (Neumann*, et al.*, 2002; Qiu*, et al.*, 2002), and in *C. elegans*, cAMP signaling triggers conditioned regeneration (Chung*, et al.*, 2016). Thus, cAMP may contribute to conditioned regeneration in part via *trx-1* activation through its CRE region.

Using our fluorescence proxy, we isolated twelve mutant lines with significantly decreased ASJ fluorescence. Six of those lines display significantly reduced ectopic outgrowth, which is related to conditioned regeneration, indicating that they contain a mutation in the conditioning pathways. Additionally, we developed a fluorescent bead normalization protocol to facilitate quantitative comparison of fluorescence in genetic backgrounds or under different interventions. These tools enable us to pursue a rapid, yet quantitative approach to the question of neuronal regeneration. Our approach is complimentary to established techniques for identifying RAGs, such as microarray analysis (Costigan*, et al.*, 2002). In contrast to these RAGs, genes identified by our approach are highly likely to functionally underlie regeneration, by virtue of their involvement in ectopic outgrowth.

Our proxy demonstrates significant potential as we isolated several strains with reduced outgrowth potential by selecting for reduced ASJ fluorescence. However, we did identify equally as many dim strains without reduced outgrowth potential (Fig. 4d). These findings are not unexpected since we introduce stochastic mutations throughout the genome and screen with a fluorescent indicator that only roughly corresponds with regenerative capacity. False positives can be a common drawback to forward genetic screens under mutagenesis due to their stochastic nature. In these isolated lines, we expect that EMS disrupted pathways directly related to *trx-1* expression, genes that interact upstream of *trx-1*, or the transgenic label itself, thus causing a significant reduction in fluorescence. These effects can be mitigated by pursuing a reverse genetic screen under RNAi to test genes that have an expected role in conditioned

regeneration. A similar screen was successfully carried out on transcription factors regulating non-conditioned *trx-1* expression (Gonzalez-Barrios*, et al.*, 2015).

Additionally, we screen for decreased fluorescence by eye under the current workflow. This reduction in fluorescence is often difficult to distinguish by eye. Also, the range of fluorescence of the starting strain and mutant often overlap, which prevented outcrossing and identification of the causative mutations. We could improve the throughput and probability of success by implementing real-time quantitative measurements to more precisely screen for changes in fluorescence. For instance, we could utilize microfluidic devices to rapidly screen through animals for a reduction in fluorescence or implement whole plate imaging to quickly image entire populations of animals to select for decreased fluorescence.

Outlook

Studying regeneration *in vivo* remains difficult for experimental reasons and due to interacting pathways yet to be explored and fully defined. We have developed a single-cell model to study the conventional and conditioned regeneration pathways in the *C. elegans* ASJ neuron and a proxy to identify genes and potential therapeutic targets involved. Our study could be extended in multiple directions. First, the mechanisms through which *trx-1* (and potentially its redox activities) modulates regeneration remain unclear. This direction is of particular interest because *trx-1* specifically enhances conditioned, but inhibits conventional, regeneration. Second, the mechanisms that underlie *trx-1* expression and their relation to conditioning pathways should be clarified. Third, while *trx-1* expression is specific to the ASJ, our approach could be extended to

other neurons by labeling with fluorescent reporters driven by their RAGs. Neuron types and even subtypes have distinct regeneration capacities (Duan*, et al.*, 2015), but broad regeneration studies in multiple neurons are lacking. Examining regeneration in other neurons may illuminate new regeneration pathways. Our work thus represents an important first step in identifying undiscovered modulators of neuron regeneration and in establishing new approaches for rapidly studying regeneration.

Acknowledgements

We thank members of the Chung laboratory for taking part in the revision process. We acknowledge Peter Swoboda (Karolinska Institute, Huddinge, Sweden) for providing OE3417 and Antonio Miranda-Vizuete (Biomedicine Institute of Sevilla, Seville, Spain) for providing VZ763 and comments on the manuscript.

References

Bai, J., Nakamura, H., Kwon, Y.W., Hattori, I., Yamaguchi, Y., Kim, Y.C., Kondo, N., Oka, S., Ueda, S., Masutani, H.*, et al.* (2003). Critical roles of thioredoxin in nerve growth factor-mediated signal transduction and neurite outgrowth in PC12 cells. J Neurosci *23*, 503-509.

Brenner, S. (1974). The genetics of Caenorhabditis elegans. Genetics *77*, 71-94.

Chong, M.S., Woolf, C.J., Turmaine, M., Emson, P.C., and Anderson, P.N. (1996). Intrinsic versus extrinsic factors in determining the regeneration of the central processes of rat dorsal root ganglion neurons: The influence of a peripheral nerve graft. J Comp Neurol *370*, 97-104.

Chung, S.H., Awal, M.R., Shay, J., McLoed, M.M., Mazur, E., and Gabel, C.V. (2016). Novel DLK-independent neuronal regeneration in Caenorhabditis elegans shares links with activity-dependent ectopic outgrowth. Proc Natl Acad Sci USA *113*, E2852-E2860.

Chung, S.H., Clark, D.A., Gabel, C.V., Mazur, E., and Samuel, A.D. (2006). The role of the AFD neuron in C. elegans thermotaxis analyzed using femtosecond laser ablation. BMC Neurosci *7*, 30.

Coburn, C.M., and Bargmann, C.I. (1996). A putative cyclic nucleotide-gated channel is required for sensory development and function in C. elegans. Neuron *17*, 695-706.

Costigan, M., Befort, K., Karchewski, L., Griffin, R.S., D'Urso, D., Allchorne, A., Sitarski, J., Mannion, J.W., Pratt, R.E., and Woolf, C.J. (2002). Replicate high-density rat genome oligonucleotide microarrays reveal hundreds of regulated genes in the dorsal root ganglion after peripheral nerve injury. BMC Neurosci *3*.

Duan, X., Qiao, M., Bei, F., Kim, I.-J., He, Z., and Sanes, Joshua R. (2015). Subtype-Specific Regeneration of Retinal Ganglion Cells following Axotomy: Effects of Osteopontin and mTOR Signaling. Neuron *85*, 1244-1256.

Dubový, P., Klusáková, I., Hradilová-Svíženská, I., Brázda, V., Kohoutková, M., and Joukal, M. (2019). A Conditioning Sciatic Nerve Lesion Triggers a Pro-regenerative State in Primary Sensory Neurons Also of Dorsal Root Ganglia Non-associated With the Damaged Nerve. Front Cell Neurosci *13*.

Feigin, V.L., Vos, T., Alahdab, F., Amit, A.M.L., Bärnighausen, T.W., Beghi, E., Beheshti, M., Chavan, P.P., Criqui, M.H., Desai, R.*, et al.* (2021). Burden of Neurological Disorders Across the US From 1990-2017. JAMA Neurology *78*, 165.

Franz, C.K., Quach, E.T., Krudy, C.A., Federici, T., Kliem, M.A., Snyder, B.R., Raore, B., and Boulis, N.M. (2009). A Conditioning Lesion Provides Selective Protection in a Rat Model of Amyotrophic Lateral Sclerosis. PLOS ONE *4*, 8.

Ghosh-Roy, A., Wu, Z.L., Goncharov, A., Jin, Y.S., and Chisholm, A.D. (2010). Calcium and Cyclic AMP Promote Axonal Regeneration in Caenorhabditis elegans and Require DLK-1 Kinase. J Neurosci *30*, 3175-3183.

Gonzalez-Barrios, M., Fierro-Gonzalez, J.C., Krpelanova, E., Mora-Lorca, J.A., Pedrajas, J.R., Penate, X., Chavez, S., Swoboda, P., Jansen, G., and Miranda-Vizuete, A. (2015). Cis- and Trans-Regulatory Mechanisms of Gene Expression in the ASJ Sensory Neuron of Caenorhabditis elegans. Genetics *200*, 123-U269.

Hammarlund, M., Nix, P., Hauth, L., Jorgensen, E.M., and Bastiani, M. (2009). Axon Regeneration Requires a Conserved MAP Kinase Pathway. Science *323*, 802-806.

Harreguy, M.B., Marfil, V., Grooms, N.W.F., Gabel, C.V., Chung, S.H., and Haspel, G. (2020). Ytterbium-doped fibre femtosecond laser offers robust operation with deep and precise microsurgery of C. elegans neurons. Sci Rep *10*, 4545.

Hoffman, P.N. (2010). A conditioning lesion induces changes in gene expression and axonal transport that enhance regeneration by increasing the intrinsic growth state of axons. Exp Neurol *223*, 11-18.

Itoh, A., Horiuchi, M., Bannerman, P., Pleasure, D., and Itoh, T. (2009). Impaired regenerative response of primary sensory neurons in ZPK/DLK gene-trap mice. Biochemical and Biophysical Research Communications *383*, 258-262.

James, S.L., Theadom, A., Ellenbogen, R.G., Bannick, M.S., Montjoy-Venning, W., Lucchesi, L.R., Abbasi, N., Abdulkader, R., Abraha, H.N., Adsuar, J.C.*, et al.* (2019). Global, regional, and national burden of traumatic brain injury and spinal cord injury, 1990–2016: a systematic analysis for the Global Burden of Disease Study 2016. The Lancet Neurology *18*, 56-87.

Kim, K.W., Tang, N.H., Piggott, C.A., Andrusiak, M.G., Park, S., Zhu, M., Kurup, N., Cherra, S.J., Wu, Z., Chisholm, A.D.*, et al.* (2018). Expanded genetic screening in Caenorhabditis elegans identifies new regulators and an inhibitory role for NAD+ in axon regeneration. eLife *7*.

Ma, T.C., and Willis, D.E. (2015). What makes a RAG regeneration associated? Front Mol Neurosci *8*, 13.

Mansur, K., Iwahashi, Y., Kiryu-Seo, S., Su, Q., Namikawa, K., Yodoi, J., and Kiyama, H. (1998). Up-regulation of thioredoxin expression in motor neurons after nerve injury. Mol Brain Res *62*, 86-91.

McQuarrie, I.G., and Grafstein, B. (1973). Axon Outgrowth Enhanced by a Previous Nerve Injury. Arch Neurol *29*, 53-55.

Miranda-Vizuete, A., Gonzalez, J.C., Gahmon, G., Burghoorn, J., Navas, P., and Swoboda, P. (2006). Lifespan decrease in a Caenorhabditis elegans mutant lacking TRX-1, a thioredoxin expressed in ASJ sensory neurons. FEBS Lett *580*, 484-490.

Neumann, S., Bradke, F., Tessier-Lavigne, M., and Basbaum, A.I. (2002). Regeneration of sensory axons within the injured spinal cord induced by intraganglionic cAMP elevation. Neuron *34*, 885-893.

Oudega, M., Varon, S., and Hagg, T. (1994). Regeneration of Adult Rat Sensory Axons into Intraspinal Nerve Grafts: Promoting Effects of Conditioning Lesion and Graft Predegeneration. Exp Neurol *129*, 194-206.

Peckol, E.L., Zallen, J.A., Yarrow, J.C., and Bargmann, C.I. (1999). Sensory activity affects sensory axon development in C. elegans. Development *126*, 1891-1902.

Qiu, J., Cai, C.M., Dai, H.N., McAtee, M., Hoffman, P.N., Bregman, B.S., and Filbin, M.T. (2002). Spinal axon regeneration induced by elevation of cyclic AMP. Neuron *34*, 895-903.

Richardson, P.M., and Issa, V.M.K. (1984). Peripheral Injury Enhances Central Regeneration of Primary Sensory Neurons. Nature *309*, 791-793.

Shin, J.E., Cho, Y.C., Beirowski, B., Milbrandt, J., Cavalli, V., and DiAntonio, A. (2012). Dual Leucine Zipper Kinase Is Required for Retrograde Injury Signaling and Axonal Regeneration. Neuron *74*, 1015-1022.

Stemme, S., Hansson, H.A., Holmgren, A., and Rozell, B. (1985). Axoplasmic transport of thioredoxin and thioredoxin reductase in rat sciatic nerve. Brain Res *359*, 140-146.

474 Stenvall, J., Fierro-González, J.C., Swoboda, P., Saamarthy, K., Cheng, Q., Cacho-
475 Valadez, B., Arnér, E.S.J., Persson, O.P., Miranda-Vizuete, A., and Tuck, S. (2011).
476 Selenoprotein TRXR-1 and GSR-1 are essential for removal of old cuticle during molting
477 in *Caenorhabditis elegans*. Proceedings of the National Academy of Sciences *108*,
478 1064-1069.
479 Sugino, T., Nozaki, K., Takagi, Y., Hattori, I., Hashimoto, N., and Yodoi, J. (1999).
480 Expression and distribution of redox regulatory protein, thioredoxin after metabolic
481 impairment by 3-nitropropionic acid in rat brain. Neurosci Lett *275*, 145-148.
482 Takagi, Y., Mitsui, A., Nishiyama, A., Nozaki, K., Sono, H., Gon, Y., Hashimoto, N., and
483 Yodoi, J. (1999). Overexpression of thioredoxin in transgenic mice attenuates focal
484 ischemic brain damage. Proceedings of the National Academy of Sciences *96*, 4131-
485 4136.
486 Tomimoto, H., Akiguchi, I., Wakita, H., Kimura, J., Hori, K., and Yodoi, J. (1993).
487 Astroglial expression of ATL-derived factor, a human thioredoxin homologue, in the
488 gerbil brain after transient global ischemia. Brain Res *625*, 1-8.
489 Wang, Y.L., Grooms, N.W.F., and Chung, S.H. (2022). Transverse and axial resolution
490 of femtosecond laser ablation. J Biophotonics, e202200042.
491 White, J.G., Southgate, E., Thomson, J.N., and Brenner, S. (1986). The structure of the
492 nervous system of the nematode Caenorhabditis elegans. Philos Transact B-Biol Sci
493 *314*, 1-340.
494 Xiong, X., and Collins, C.A. (2012). A conditioning lesion protects axons from
495 degeneration via the Wallenda/DLK MAP kinase signaling cascade. J Neurosci *32*, 610-
496 615.
497

498

interventions →	condition neuron → phenotype
surgery conditioning mutations pharmacology	regeneration ectopic outgrowth **fluorescence**

Table 1: Interventions condition neurons by disrupting sensory signaling. Conditioning generates visible phenotypes. We examine *trx-1::gfp* fluorescence in this study.

mutation	translational marker		transcriptional marker
	ofIs1[ptrx-1::trx-1::gfp]	*ofIs4[ptrx-1::trx-1::gfp]*	*ofIs5[ptrx-1::gfp]*
none	BOS2	OE3417	BOS41
dlk-1(ju476)I	BOS71		BOS44
dlk-1(ju476)I; trx-1(ok1449)II			BOS42
egl-19(n582)IV		BOS70	
sax-1(ky211)X	BOS74		
tax-2(p691)I	BOS72	BOS76	
tax-4(p678)III		BOS73	
trx-1(ok1449)II			VZ763
unc-36(e251)III	BOS69		
unc-43(n1186n498)IV		BOS75	

Table 2: Strains and genotypes utilized.

Figure captions

Figure 1: Sensory mutations upregulate ASJ neuron expression of *trx-1*. (a) Leftmost panels: typical ASJ neuron and line drawing. Remainder of panels: representative images of *ptrx-1::trx-1::gfp* in wild-type (wt), mutant backgrounds. Sensory mutations, particularly *tax-2* and *tax-4*, upregulate expression. Identical brightness, contrast for all images except leftmost. Fluorescent bead indicated by #. (b) Quantification of fluorescence in part A. Data represented as average ± standard deviation (SD). $n = 50$ for each data point. ** $p < 0.001$

Figure 2: Dendrite cuts upregulate *trx-1* expression and condition ASJ to regenerate. (a) GFP fluorescence images of ASJ neuron. Fluorescent bead indicated by #. Identical brightness, contrast for all images. (b) Quantification of fluorescence in part A. Data represented as average ± SD. Each dot represents one animal. (c) ASJ cell body and dendrite fluorescence distributions from part B. Dendrite cut brightens fluorescence in entire population. (d) Total length of ASJ regeneration following axon or axon+dendrite (a+d) cut in wt, *dlk-1*. Dendrite cut enhances ASJ regeneration under DLK-independent mechanism. Arrows represent conditioning effect, or contribution of conditioning to additional regenerated length from dendrite cut. Data represented as average ± standard error of the mean (SEM). $n \geq 20$ for all conditions. ** $p < 0.001$. Control and *tax-2* images and data replicated from Fig. 1.

Figure 3: TRX-1 modulates ASJ regeneration. Total length of ASJ regeneration depends on genetic background and surgery type. Mutation of TRX-1 enhances

regeneration after axotomy. Conditioning effect in *dlk-1; trx-1* animals significantly reduced compared to *dlk-1* animals. Arrows represent conditioning effect. Data represented as average ± SEM. $n \geq 20$ for all conditions. * $p < 0.05$, ** $p < 0.001$.

Figure 4: Fluorescence proxy enables isolation of mutants with reduced conditioned regenerative potential. (a) ASJ images in control and post-mutagenesis animals. Fluorescent bead indicated by #. Identical brightness, contrast for all images. (b) Quantification of cell body fluorescence in part A. Reduced fluorescence in 11 mutant lines. (c) Quantification of dendrite fluorescence in part A. Reduced fluorescence in 11 mutant lines. (d) Ectopic outgrowth frequency for control and post-mutagenesis strains. Reduced ectopic outgrowth in 6 lines. Fluorescence measurements: $n = 50$. Ectopic outgrowth: $60 \leq n \leq 94$ for strains 3b, 6a, 6c; $n \geq 150$ for other strains. Strain 4a not viable at cultivation temperature. Data represented as average ± SD. * $p < 0.05$, ** $p < 0.001$. Control (*tax-2*) images and fluorescence data from Fig. 1.

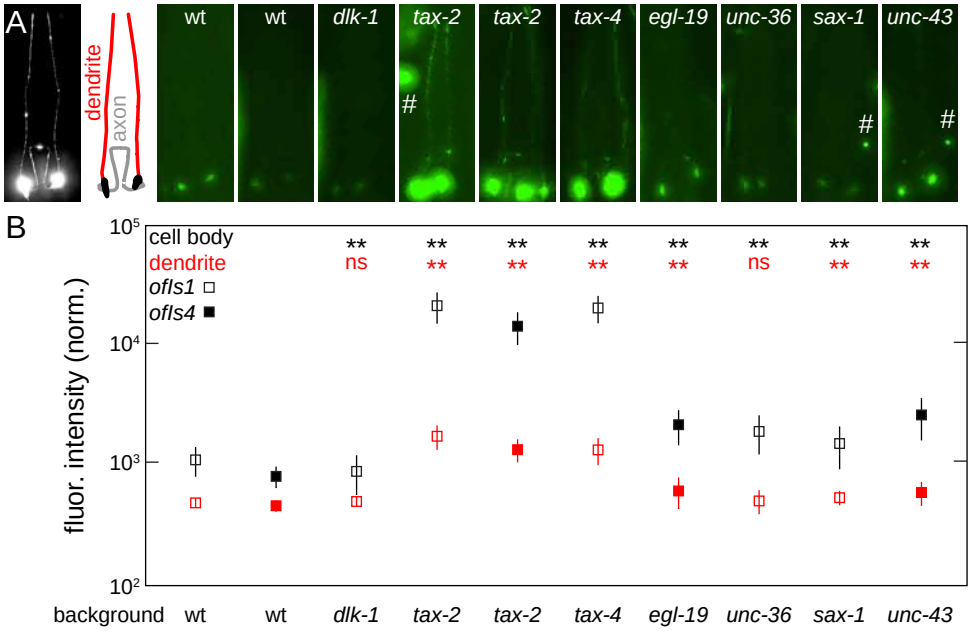

Figure 1
Grooms, et al

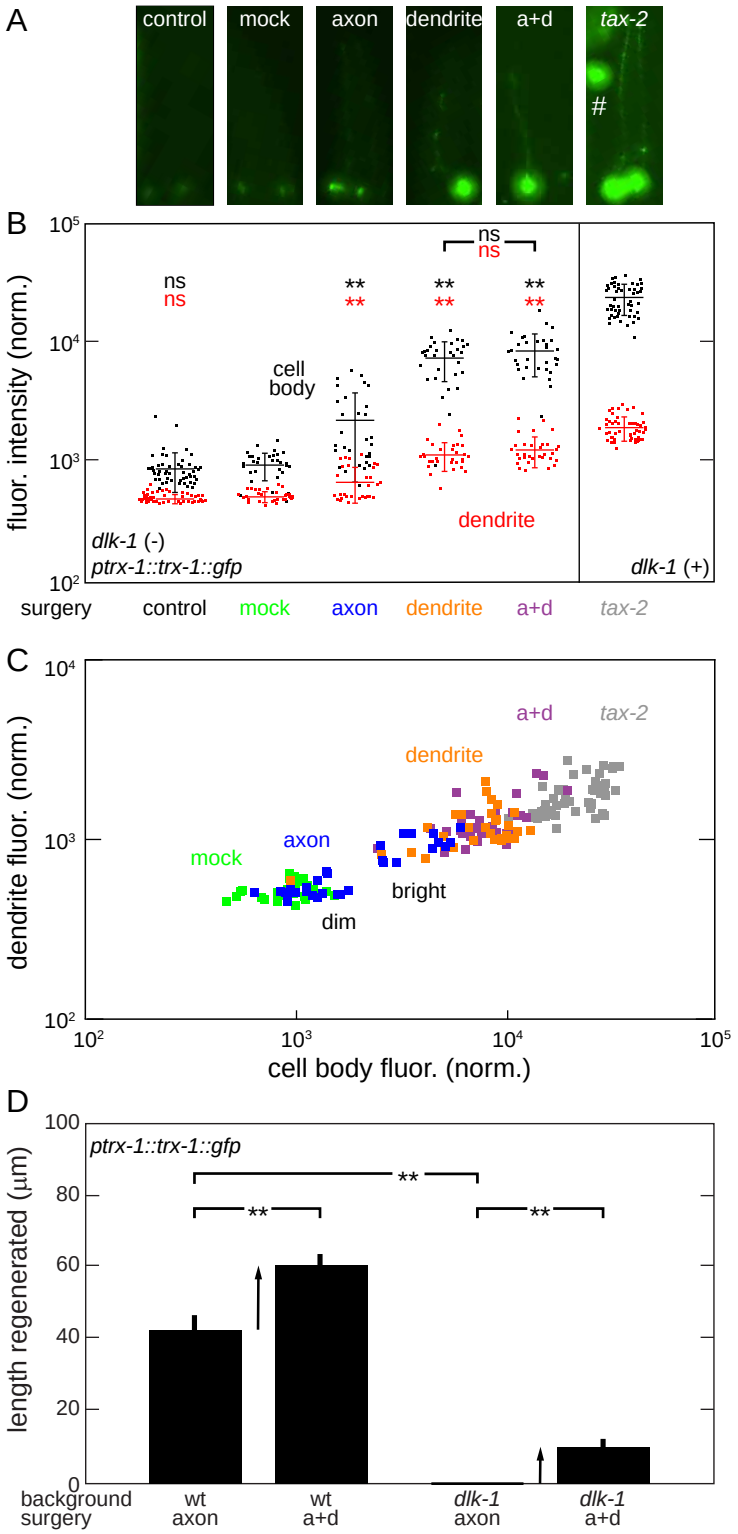

Figure 2
Grooms, et al

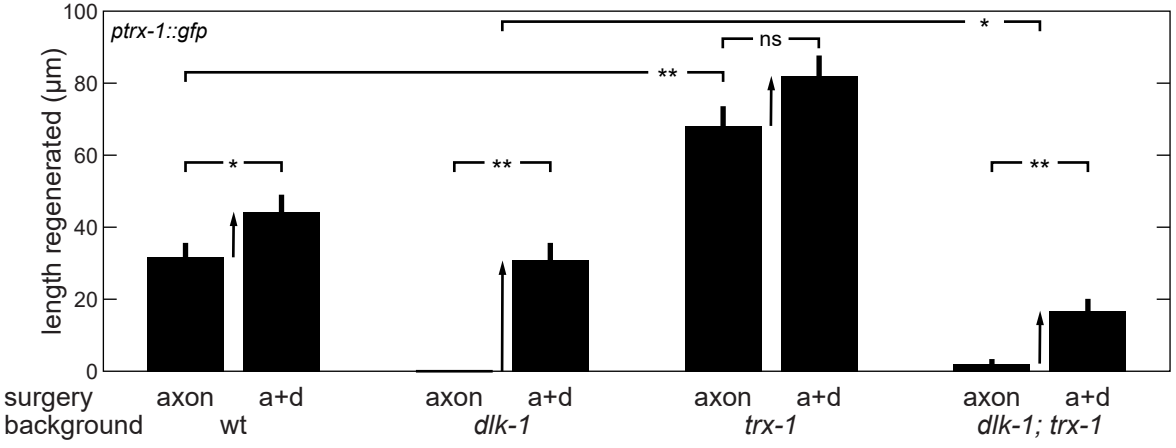

Figure 3
Grooms, et al

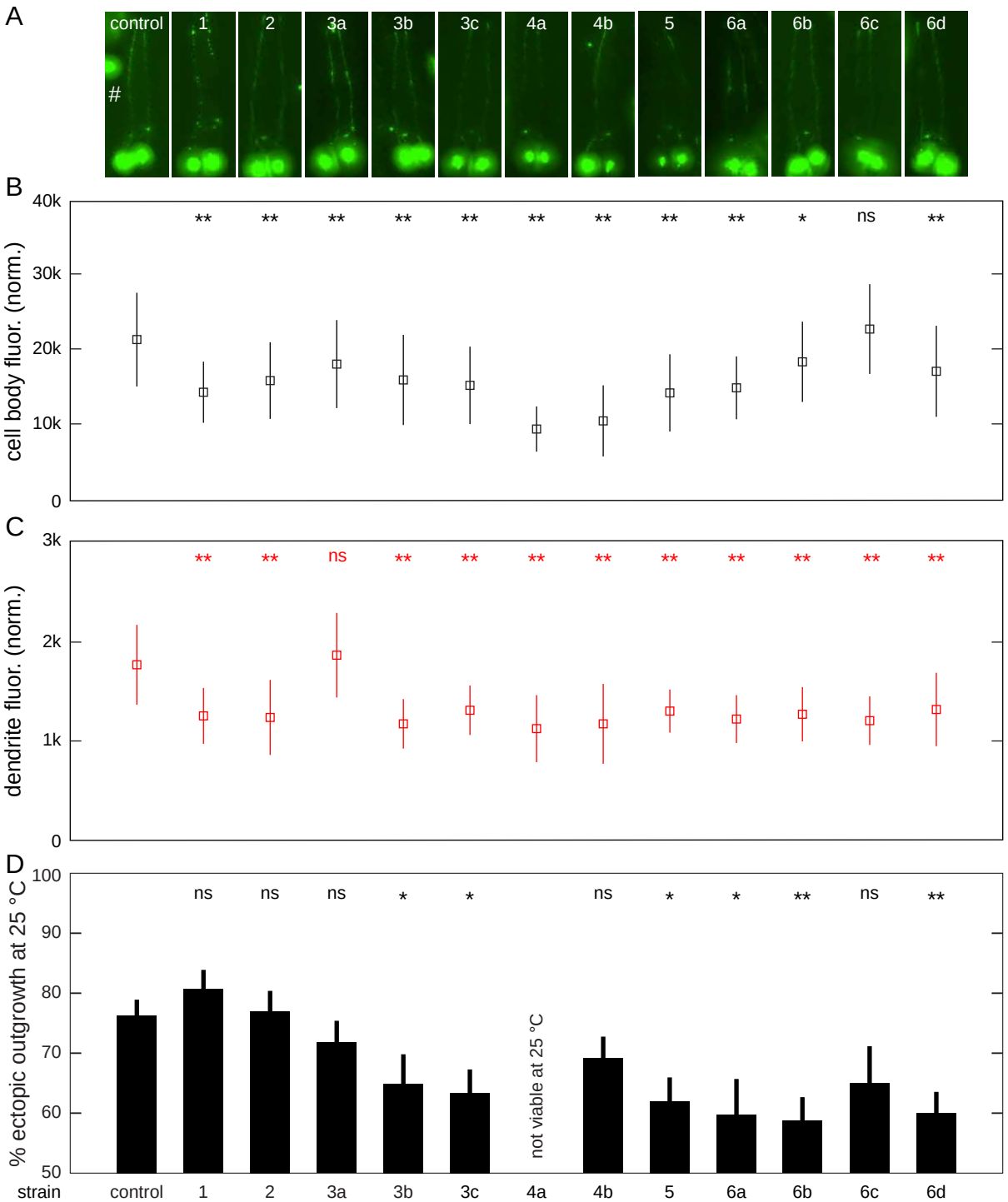

Figure 4
Grooms, et al